Supporting Information

Strain-Induced Self-Rolling of Electrochemically Deposited $Co(OH)_2$ Films into Organic–Inorganic Microscrolls

Jonas Schwan[1], Sabine Rosenfeldt[2,3], and Anna S. Schenk[1,3,*]

[1] *Physical Chemistry – Colloidal Systems, Department of Chemistry, University of Bayreuth, Universitaetsstrasse 30, 95447 Bayreuth, Germany*

[2] *Physical Chemistry I, Department of Chemistry, University of Bayreuth, Universitaetsstrasse 30, 95447 Bayreuth, Germany*

[3] *Bavarian Polymer Institute, University of Bayreuth, Universitaetsstrasse 30, 95447 Bayreuth, Germany*

** Correspondence: anna.schenk@uni-bayreuth.de*

Supplementary Data and Analyses:

Calculations:

Calculations of the Potentials for the Hydroxide Generating Electrochemical Reactions

Figures:

Figure S1 Digital light microscopy imaging of $Co(OH)_2$/PSS (PSS) microscrolls
Figure S2 Scanning electron micrographs of individual $Co(OH)_2$/PSS microscrolls
Figure S3 Comparison of film cross sections in the absence and presence of (PSS)
Figure S4 Small angle X-ray scattering patterns for non-scrolled $Co(OH)_2$ films and $Co(OH)_2$/PSS microscrolls
Figure S5 X-ray diffractograms of $Co(OH)_2$/PSS microscrolls prior to and after thermal treatment
Figure S6 Representative Raman spectrum of a selected $Co(OH)_2$/PSS microscroll
Figure S7 Confocal Raman microscopy line scan along the cross-section of an individual $Co(OH)_2$/PSS microscroll
Figure S8 Comparison of OER performance of additive-free $Co(OH)_2$ films as deposited and after pseudomorphic conversion into Co_3O_4 films
Figure S9 Overview of the deposition of $Co(OH)_2$/poly(allylamine hydrochloride) hybrid materials.
Figure S10 Dynamic light scattering data of aqueous PSS solutions with increasing additions of Co^{2+} ions

Calculations of the Potentials for the Hydroxide Generating Electrochemical Reactions

<u>Equation 1a:</u>

$$2\ H_2O + 2\ e^- \rightarrow 2\ OH^- + H_2 \quad E^0\ (\text{vs. NHE}) = -0.828\ \text{V @ pH 14}$$

Calculating the standard potential vs. Ag|AgCl using the Nernst equation:

$$E^0(\text{vs. Ag|AgCl}) = E(\text{vs. NHE}) - E^0_{Ag|AgCl}(\text{vs. NHE})$$

$$E^0(\text{vs. Ag|AgCl}) = E^0(\text{vs. NHE}) - \frac{0.059\ \text{V}}{2} \cdot 2 \cdot \log c(OH^-) - E^0_{Ag|AgCl}(\text{vs. NHE})$$

$$E^0(\text{vs. Ag|AgCl}) = E^0(\text{vs. NHE}) + 0.059\ \text{V} \cdot (14 - \text{pH}) - E^0_{Ag|AgCl}(\text{vs. NHE})$$

$$E^0(\text{vs. Ag|AgCl}) = -0.828\ \text{V} + 0.059\ \text{V} \cdot (14 - 3.9) - 0.205\ \text{V} = \mathbf{-0.437\ V}$$

<u>Equation 1b:</u>

$$NO_3{}^- + 7\ H_2O + 8\ e^- \rightarrow NH_4{}^+ + 10\ OH^- \qquad E^0\ (\text{vs. NHE}) = +0.01\ \text{V @ pH 14}$$

Calculating the standard potential vs. Ag|AgCl using the Nernst equation:

$$E^0(\text{vs. Ag|AgCl}) = E(\text{vs. NHE}) - E^0_{Ag|AgCl}(\text{vs. NHE})$$

$$E^0(\text{vs. Ag|AgCl}) = E^0(\text{vs. NHE}) - \frac{0.059\ \text{V}}{8} \cdot 10 \cdot \log c(OH^-) - E^0_{Ag|AgCl}(\text{vs. NHE})$$

$$E^0(\text{vs. Ag|AgCl}) = E^0(\text{vs. NHE}) + 0.059\ \text{V} \cdot \frac{10}{8} \cdot (14 - \text{pH}) - E^0_{Ag|AgCl}(\text{vs. NHE})$$

$$E^0(\text{vs. Ag|AgCl}) = +0.01\ \text{V} + 0.059\ \text{V} \cdot \frac{10}{8} \cdot (14 - 3.9) - 0.205\ \text{V} = \mathbf{+0.550\ V}$$

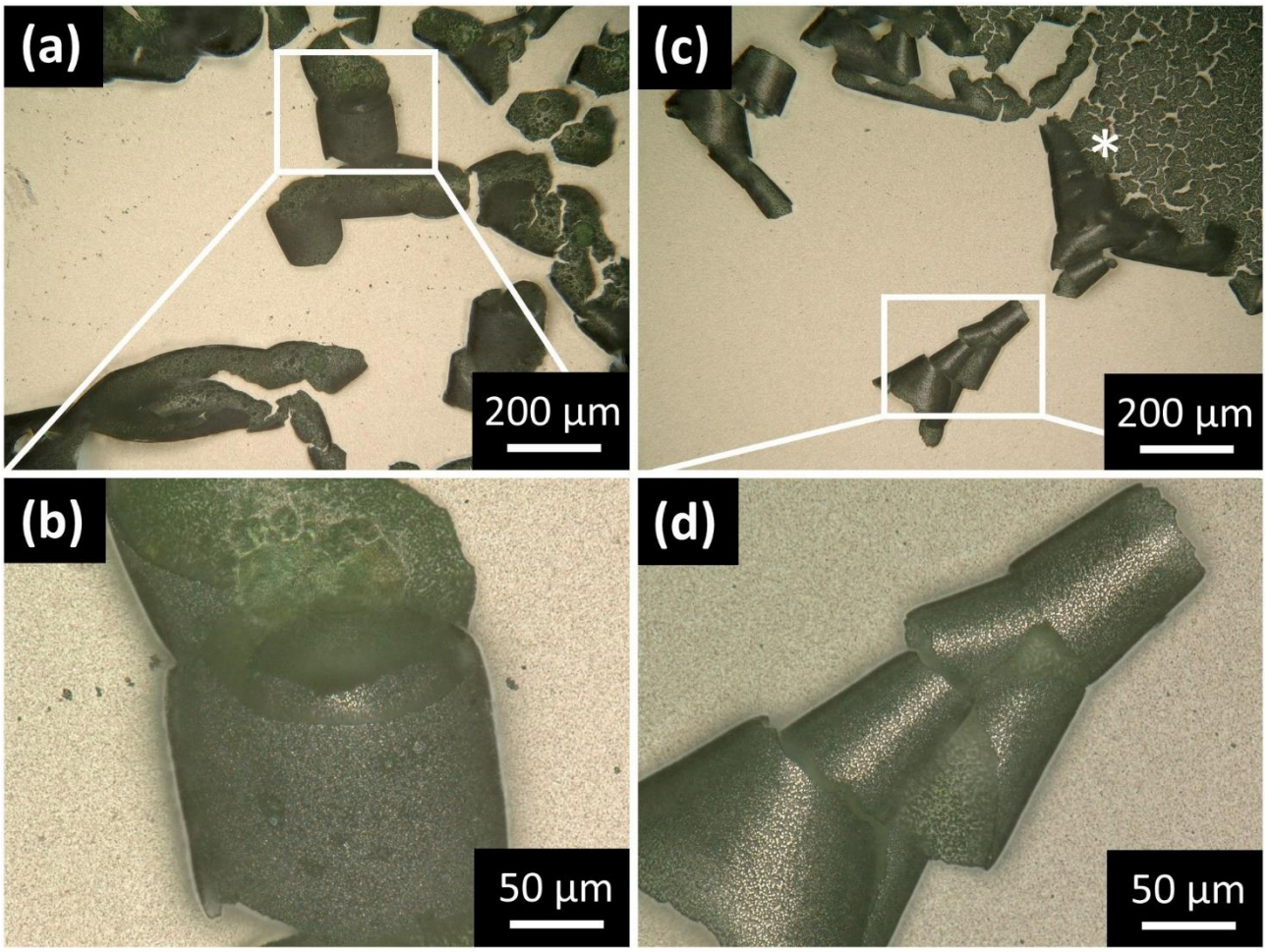

Figure S1 Digital light microscopy imaging of $Co(OH)_2$/PSS (PSS) microscrolls. (a) The continuous film fractures into fragments of irregular shape and size during air-drying at room temperature. (b) Magnified view of an individual microscroll with multiple twists. (c) Overview image showing the edge of the film rolling up towards flat fragments of the previously intact film (asterisk). (d) Magnification shows a microscroll which is irregularly curled from different directions resulting in a morphology reminiscent of an un-wound scroll.

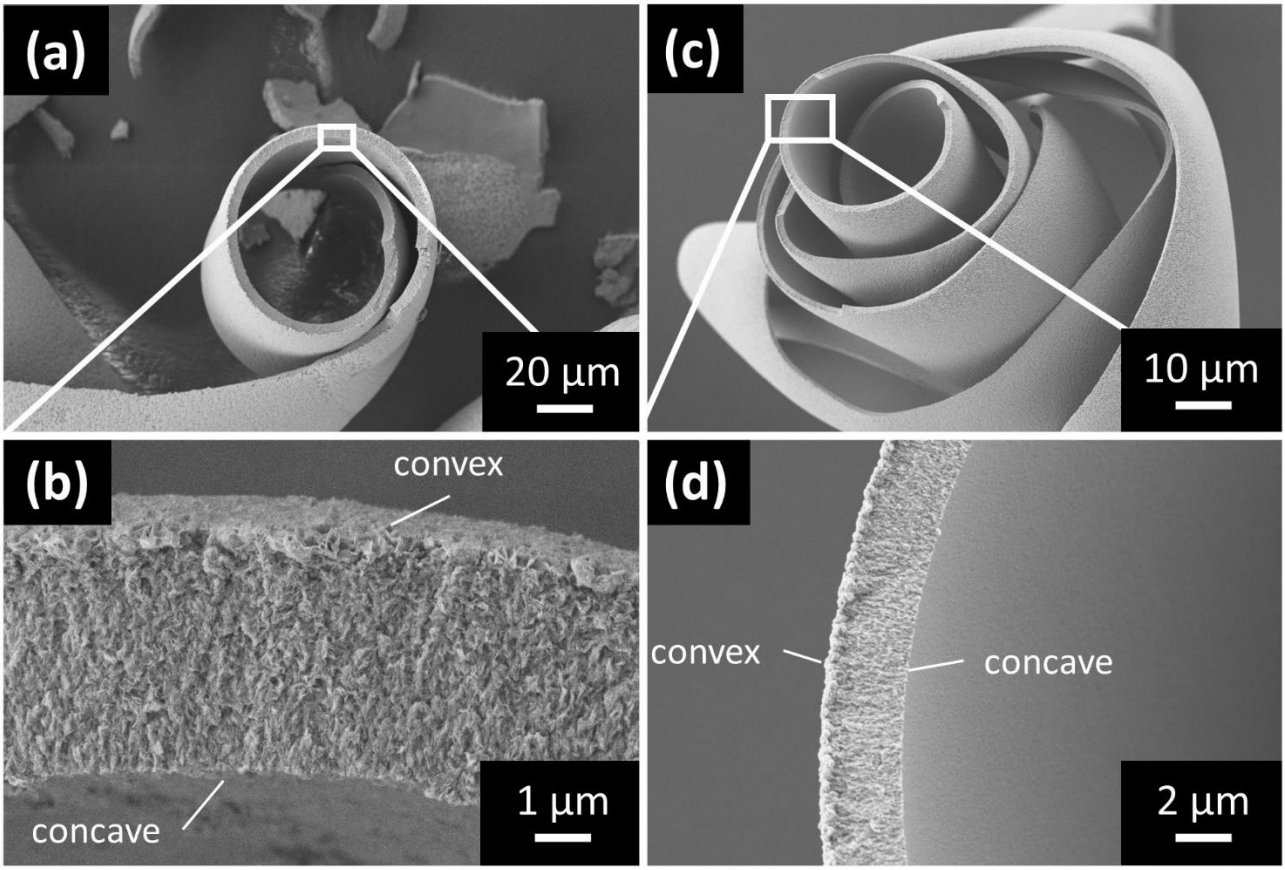

Figure S2 Scanning electron micrographs (SEM) of individual $Co(OH)_2$/PSS mircoscrolls. (a), (c) Obtained microscrolls differ in size and the number of twists. (b), (d) Magnified views reveal the bifurcated cross-section consisting of a less ordered convex and a more ordered concave surface.

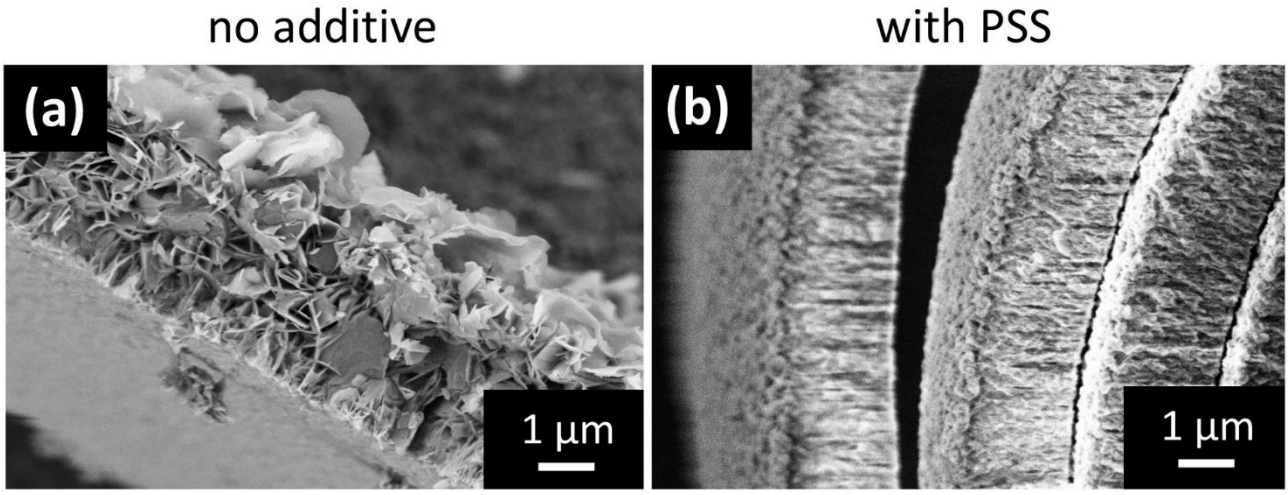

Figure S3 Comparison of film cross sections in the absence and presence of (PSS). (a) Representative flat fragment of a $Co(OH)_2$ film deposited under additive-free conditions. SEM imaging shows a mesostructure of irregularly arranged thin mineral platelets. (b) $Co(OH)_2$/PSS hybrid material with spiral morphology (*cf.* Fig. 3 in manuscript). SEM imaging reveals nanoscale granularity throughout the coiled film. A less ordered convex and a more ordered concave surface are seen in cross-sectional views of the microscroll's individual layers.

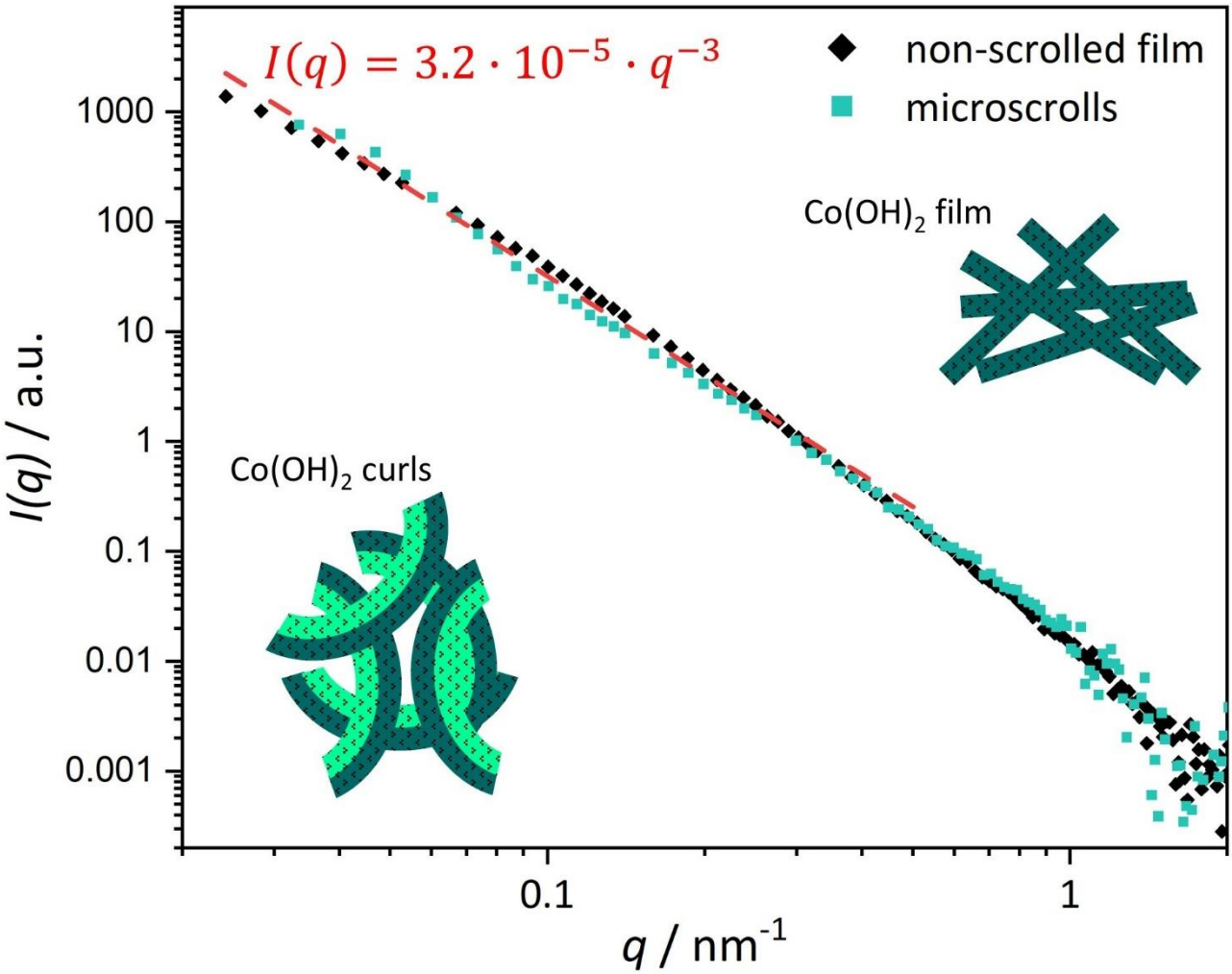

Figure S4 Small-angle X-ray scattering patterns for additive-free non-scrolled $Co(OH)_2$-films (black) and $Co(OH)_2$/PSS-microscrolls (green). The intensity decay scales with ca. q^{-3} (red line) which suggests the existence of internal porosity. These porous nanostructures can also be seen in the SEM images. The sample preparation produces disordered granular units, such that a scattering signal averaging over all spatial directions is obtained. Differences in the scattering pattern at low and intermediate q-values can be attributed to the influence of PSS, which is responsible for a more ordered nanostructure in the microscrolls compared to the non-scrolled films. The insets display a schematic overview of the samples.

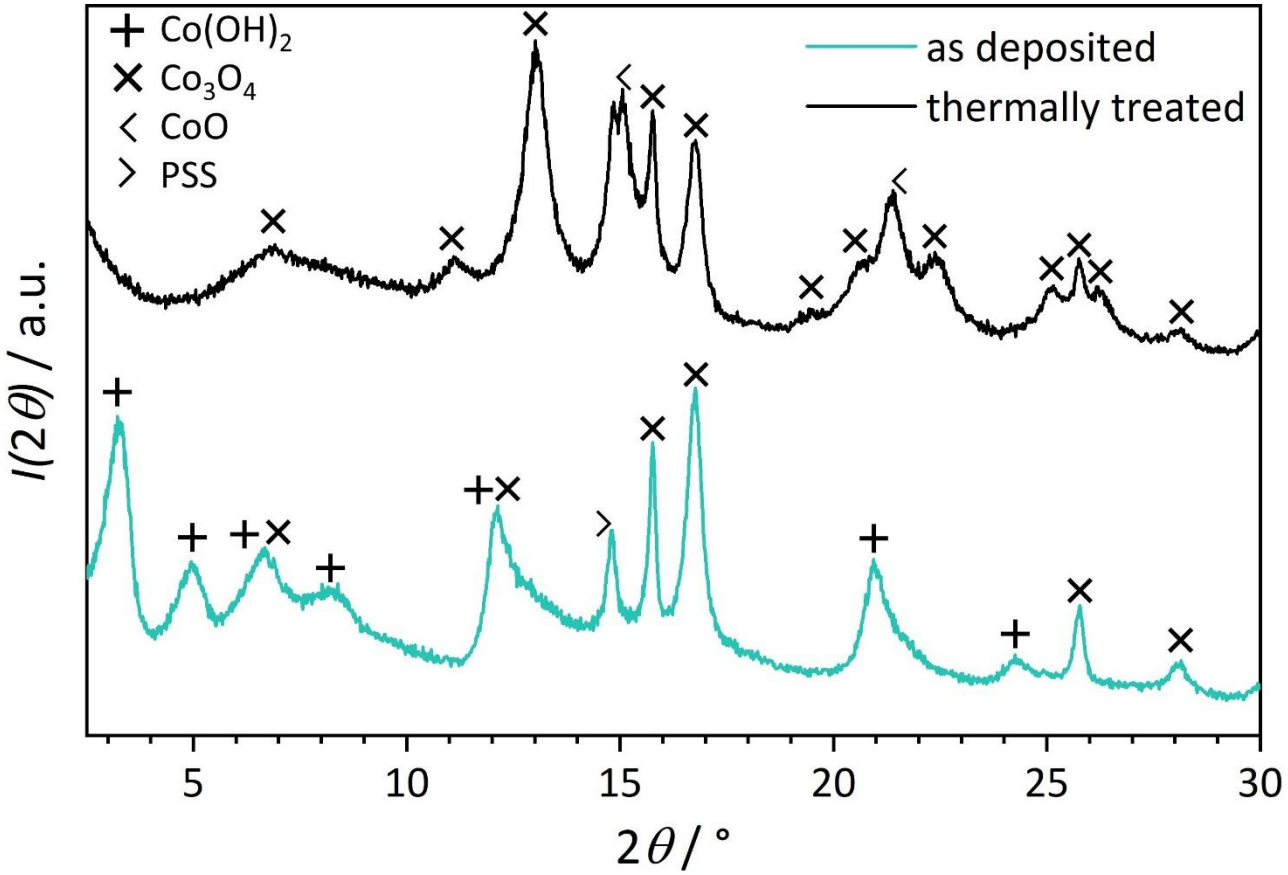

Figure S5 X-ray diffractograms of $Co(OH)_2$/PSS microscrolls prior to and after thermal treatment (300 °C for 2 h under air). For the as deposited film, most reflections can be assigned to $Co(OH)_2$ (ref. PDF 96-154-8811) while a partial oxidation in air leads to the presence of additional cobalt oxide reflections. Reflections for the 00*l* series of $Co(OH)_2$ (2θ = 3.3°, 4.9°, 6.7°, 8.2°) correspond to an interlayer spacing of d_{003} = 9.8 Å which, in combination with the green colour of the film, suggests the presence of the α-$Co(OH)_2$ phase. The incorporation of PSS is evidenced by a reflection at 2θ = 14.8°. The thermally treated microscrolls exhibit reflections mostly attributable to Co_3O_4. Thus, the data show a successful thermal conversion of α-$Co(OH)_2$/PSS microscrolls into Co_3O_4 microscrolls.

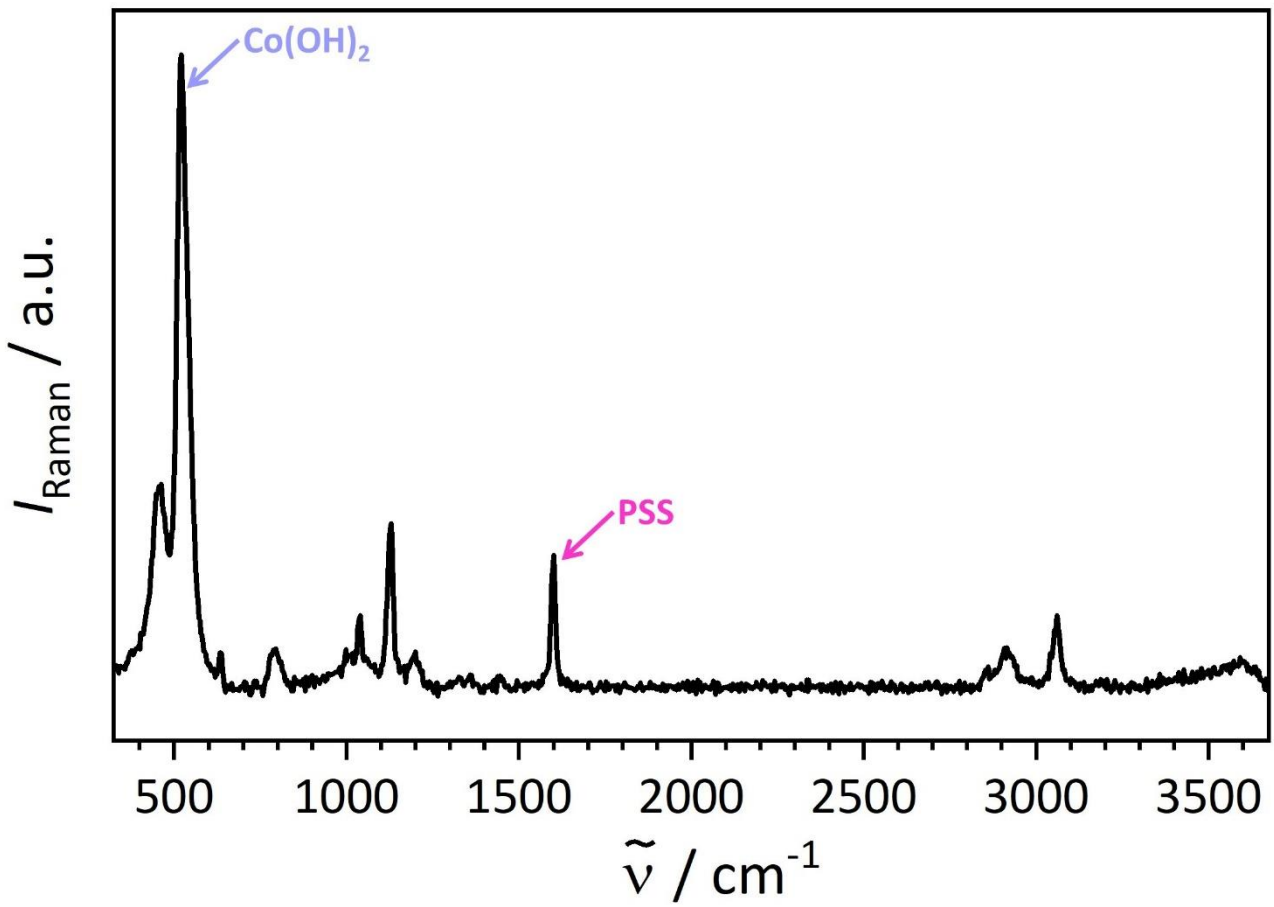

Figure S6 Representative Raman spectrum of a selected $Co(OH)_2$/PSS microscroll. The pronounced signal at 507 cm^{-1} is used for tracking the Co – O vibration intensity along the cross-section in Raman imaging experiments. The signal at 1600 cm^{-1} corresponds mainly to aromatic vibrations of PSS and is used for tracking the polymer content in microscrolls.

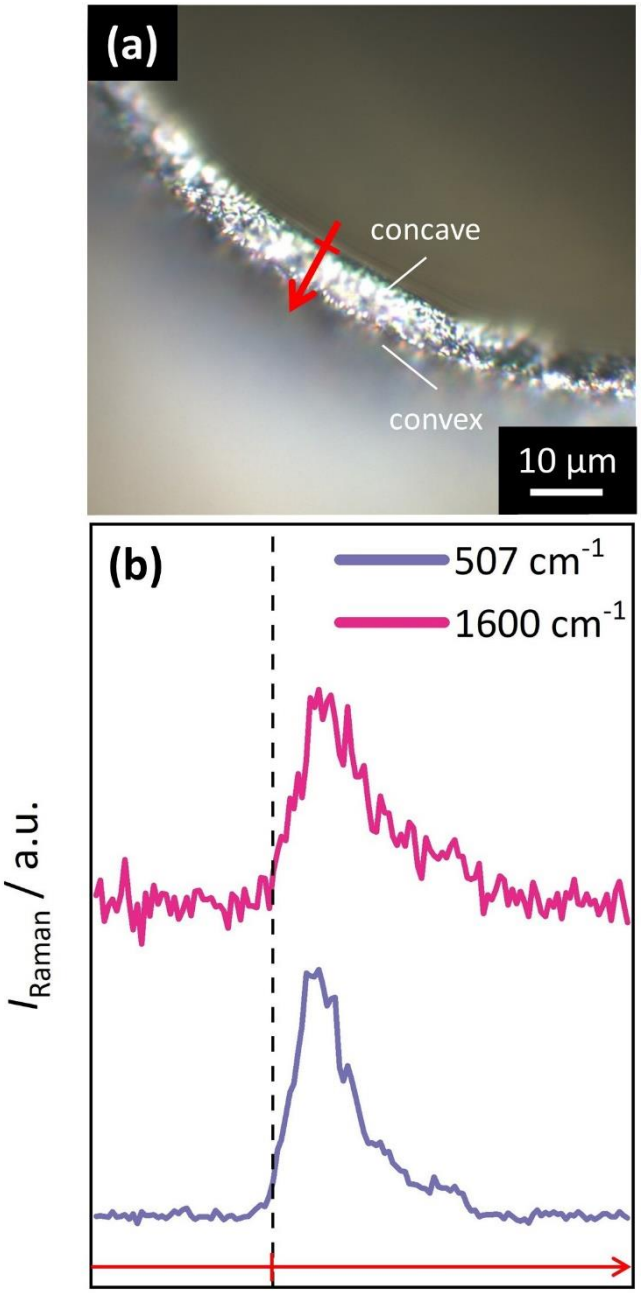

Figure S7 Confocal Raman microscopy line scan along the cross-section of an individual microscroll. (a) Optical microscopy view of the corresponding film cross-section. The red arrow marks the selected position and the direction of scanning. (b) Distribution profile of Raman intensity along the scanning direction plotted for signals corresponding to the mineral (507 cm^{-1}, Co – O vibrations; purple) and the polymer phase (1600 cm^{-1}, aromatic vibrations; pink). The dashed vertical line indicates the position of the concave surface of the microscroll with respect to the scanning direction. An overall intensity gradient of identical profile shape is visible for both signals which suggests density differences between the concave and convex surface.

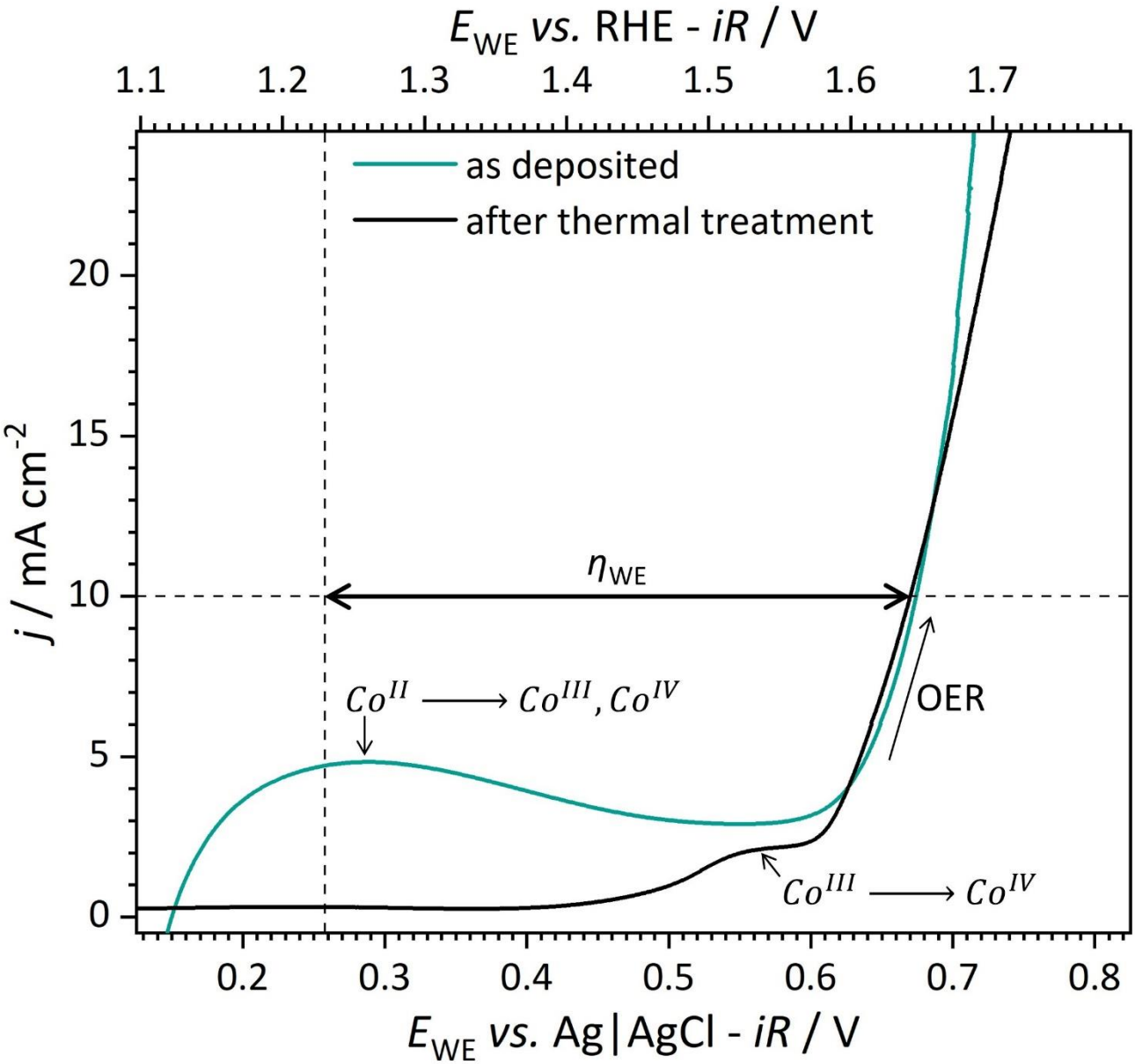

Figure S8 Comparison of OER performance of additive-free $Co(OH)_2$ films as deposited and after pseudomorphic conversion into Co_3O_4 films. The linear voltammogram recorded for $Co(OH)_2$ films (green line) shows a broad signal centered at around $E_{Ag/AgCl}$ = 270 mV corresponding to the oxidation of Co^{II} species to Co^{III} and Co^{IV}, respectively. The overpotential η_{WE} towards the oxygen evolution reaction (OER) is determined as 416 mV. The CV profile for Co_3O_4 films (black line) exhibits a more defined signal indicative of Co^{III} oxidation at $E_{Ag/AgCl}$ = 570 mV. An overpotential of η_{WE} = 412 mV towards the OER is measured.

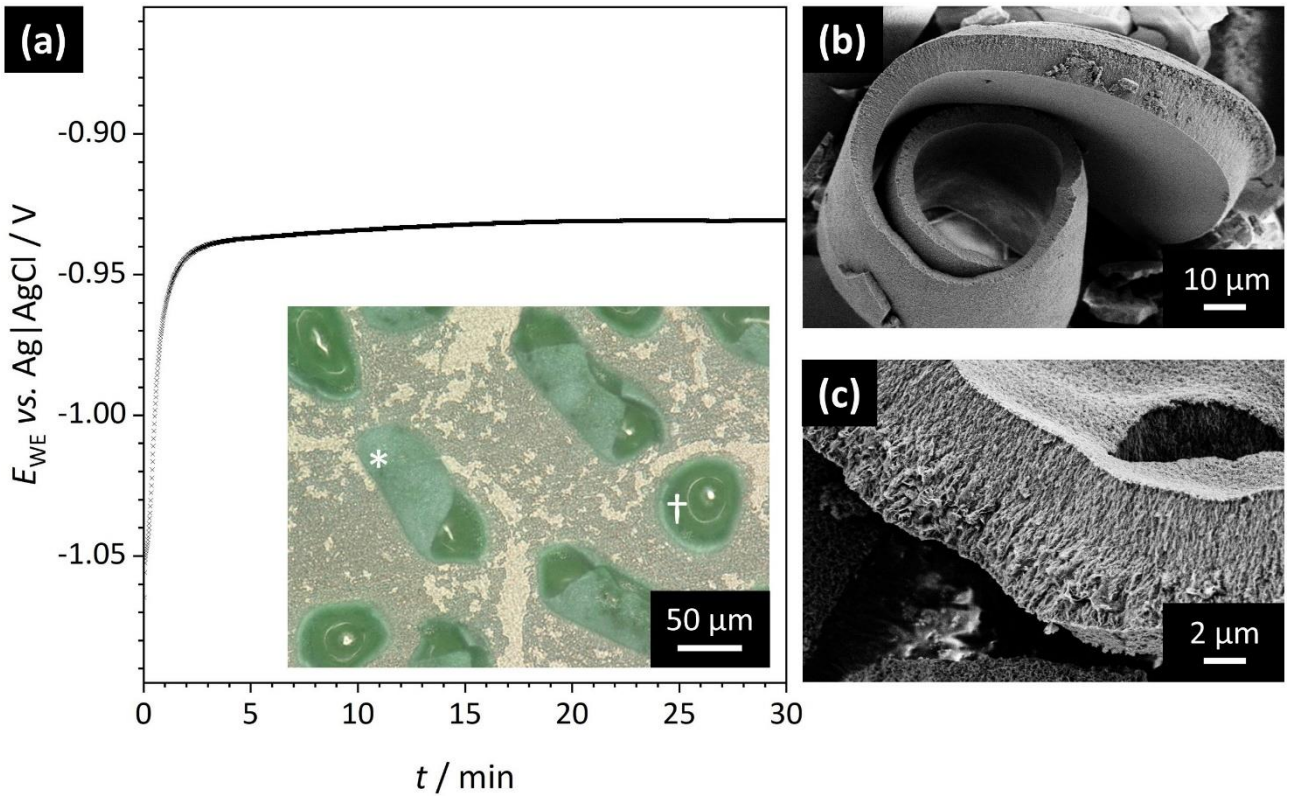

Figure S9 Overview of the deposition of $Co(OH)_2$/poly(allylamine hydrochloride) hybrid materials. (a) The electrochemical trace of the deposition process in the presence of the amine-functionalized polyelectrolyte poly(allylamine hydrochloride) (PAH) is reminiscent of the experiments with PSS (*cf.* Fig. 1 in manuscript). Inset: Digital light microscopy of obtained microscrolls exhibiting multiple twists around the principal axis (asterisk) along with curled film fragments (dagger). (b) SEM image of a representative $Co(OH)_2$/PAH microscroll with exposed cross-section. (c) A pronounced granular nanostructure is observed in cross-sectional views of the film fragments. Conspicuous heterogeneities with respect to the density and order of the nanostructural motifs between the convex and the concave side of the film result in a bilayer appearance.

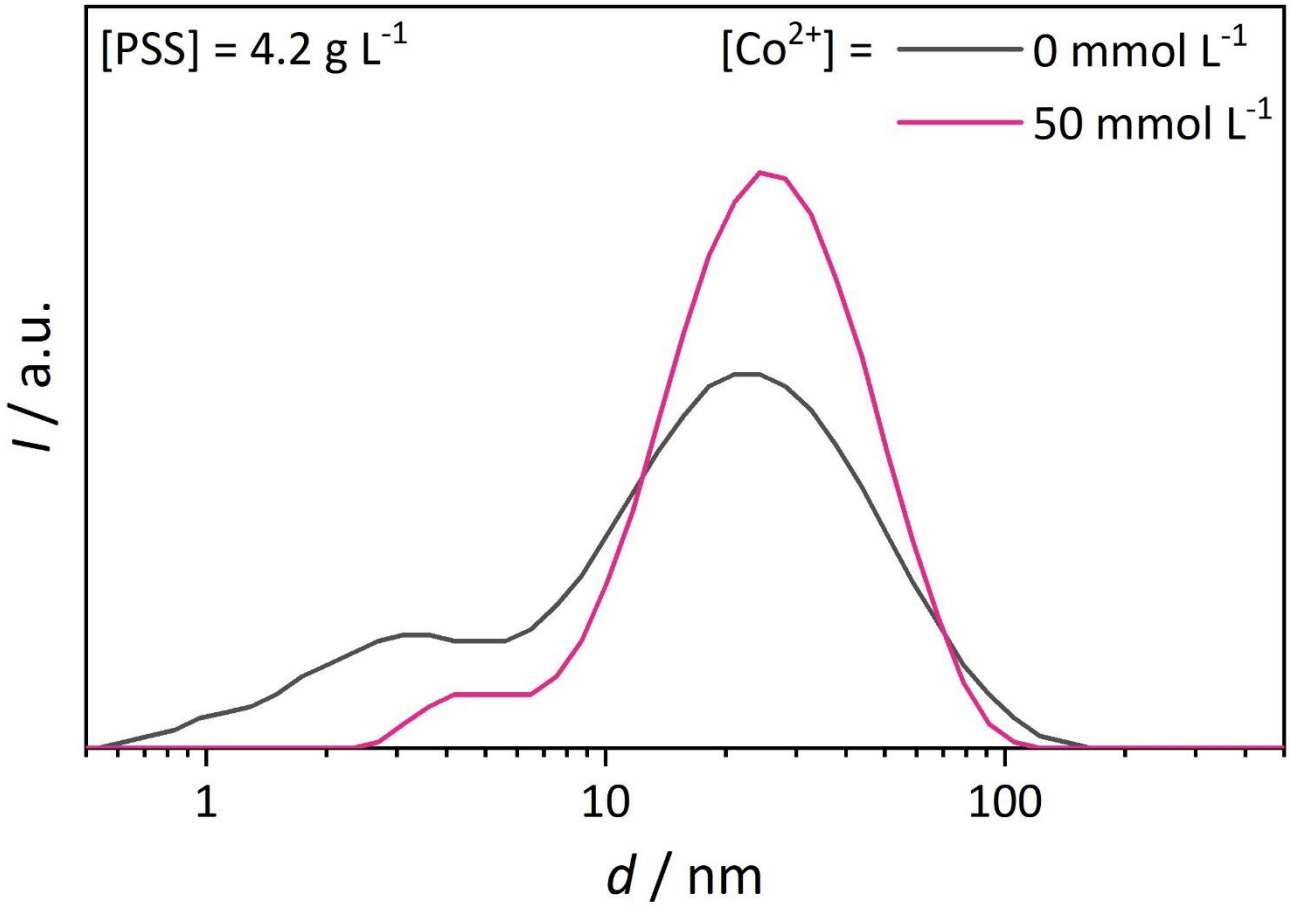

Figure S10 Dynamic light scattering data of aqueous PSS solutions ([PSS] = 4.2 g L^{-1}) with increasing additions of Co^{2+} ions. In the absence of Co^{2+} cations the size distribution of PSS species (presumably screened by residual Na^{+}) centers around two fractions with dimensions of 3 nm and 27 nm. Upon addition of Co^{2+} the relative intensity of the signal corresponding to the 27 nm sized aggregates significantly increases. The sharp and intense peak indicates an interaction between the transition metal ions and the polyelectrolyte and points to the formation of complexes in the electrolyte solution prior to the electrochemical deposition.